

Multidimensional Thermal Structure of Magnetized Neutron Star Envelopes

Jeremy S. Heyl¹

Lars Hernquist

Lick Observatory, University of California, Santa Cruz, California 95064, USA

ABSTRACT

Recently launched x-ray telescopes have discovered several candidate isolated neutron stars. The thermal radiation from these objects may potentially constrain our understanding of nuclear physics in a realm inaccessible to terrestrial experiments. To translate the observed fluxes from neutron stars into constraints, one needs precise calculations of the heat transfer through the thin insulating envelopes of neutron stars. We describe models of the thermal structure of the envelopes of neutron stars with magnetic fields up to 10^{14} G. Unlike earlier work, we infer the properties of envelope models in two dimensions and precisely account for the quantization of the electron phase space. Both dipole and uniformly magnetized envelopes are considered.

1. Introduction

Isolated neutron stars can be used as powerful tools for understanding the properties of nuclear matter. The internal structure of neutron stars spans the high-density, low-temperature regime of the QCD phase diagram which is neither constrained by terrestrial experiments such as heavy-ion collisions nor by the properties of the early universe. Both the sizes of neutron stars and their cooling evolution depend crucially on the nuclear equation of state and the species present in the stellar core. The emission that we observe from the surfaces of isolated neutron stars does give a picture of the properties of the nuclear material in the core, but it is a view through the crust of the star. Depending on the properties of the crust, the thermal flux can vary significantly for a fixed core temperature.

Fortunately, after the first few hundred years of a neutron star's life, the core becomes nearly isothermal and cooling proceeds quasistatically. During this era, the neutron star separates thermally into three regions. At the highest densities is the core which provides the thermal inertia. From densities $\rho \sim 10^{10}$ g/cm³ down to $\rho \sim 10^2$ g/cm³ is the envelope which insulates the core thermally from the exterior and which throttles the photon flux from the surface. The lowest density region is the atmosphere which effectively determines the spectrum of the neutron star but not the total flux emitted. In this paper, we focus on the properties of the envelope which will determine the gross properties of the emitted thermal radiation.

Although analytic studies (*e.g.* Heyl & Hernquist 1998; hereafter Paper I) of neutron star envelopes can well characterize the emission from cooling neutron stars, particularly those with either sufficiently weak or strong fields, most potentially observable neutron stars possess field strengths in neither of these limits and have high core temperatures which invalidate the low-temperature approximation used in Paper I.

The analytic technique outlined in Paper I assumes that only the first Landau level is filled, that the transition from the highly non-degenerate regime to the highly degenerate regime is abrupt, and

¹Current address: Theoretical Astrophysics, mail code 130-33, California Institute of Technology, Pasadena, CA 91125

that locally either electrons or photons dominate the heat transfer. In the calculations here, all three of these assumptions are relaxed, and the equations of thermal structure are integrated using opacities that approach those used in Paper I in the low and high temperature limits (Pavlov & Yakovlev 1977; Silant'ev & Yakovlev 1980; Hernquist 1984).

In Paper I several two dimensional models of neutron-star envelopes were presented. Unfortunately, the analytic separation of the structure equation requires that the two-dimensional models be restricted to cases where the entire degenerate portion of the envelope is the liquid state. Here, because the equations are solved numerically, this restriction is not important. We construct several uniformly magnetized envelopes whose thermal flux is proportional to the square of the cosine of the angle between the magnetic field and the normal, the $\cos^2 \psi$ rule proposed earlier, and verify that this distribution yields a uniform core temperature more generally. These two-dimensional results are compared with those of Schaaf (1990a) and extended to include envelopes with a dipole field structure.

Although it would be straightforward to examine additional effects such as Coulomb corrections (*e.g.* Van Riper 1988, Thorolfsson et al. 1997), for clarity and brevity only the processes included in Paper I are incorporated and the consequences of our approximations are determined.

2. The Physical Description of the Envelope

Because the assumptions made in Paper I will be relaxed, it is useful to summarize the complete set of equations governing the thermal structure of neutron star envelopes. Again, as argued earlier, a plane-parallel treatment is suitable for the problem. In what follows, use will be made of the dimensionless units

$$\beta = \frac{\hbar\omega_B}{m_e c^2} = \frac{\hbar|e|}{m_e^2 c^3} B \approx \frac{B}{4.4 \times 10^{13} \text{ G}}, \quad (1)$$

$$\tau = \frac{kT}{m_e c^2} \approx \frac{T}{5.9 \times 10^9 \text{ K}}, \quad (2)$$

$$\gamma = \frac{E}{m_e c^2} \text{ and } \zeta = \frac{\mu}{m_e c^2} \quad (3)$$

where E is the energy of an electron and μ is the chemical potential of the electron gas. It is also convenient to define $\eta = (\zeta - 1)/\tau$.

2.1. The Thermal Structure Equation

If we assume that the pressure is supplied by the electrons alone, the general relativistic equations of thermal structure in the plane-parallel approximation assume the simple form (Hernquist 1985)

$$\frac{d\tau}{d\rho} = \left[\frac{\partial \rho}{\partial \tau} \Big|_{\zeta} + \left(\frac{m_u}{Y_e} \frac{\kappa}{F/g_s} - \frac{S_e}{n_e} \right) \frac{1}{k} \frac{\partial \rho}{\partial \zeta} \Big|_{\tau} \right]^{-1} \quad (4)$$

$$\frac{d\zeta}{d\rho} = \left(\frac{\partial \rho}{\partial \zeta} \Big|_{\tau} \right)^{-1} \left(1 - \frac{\partial \rho}{\partial \tau} \Big|_{\zeta} \frac{d\tau}{d\rho} \right) \quad (5)$$

$$\frac{dz}{d\rho} = -\frac{d\zeta}{d\rho} \frac{m_e c^2}{g_s} \left(1 - \frac{F}{g_s} \frac{S_e}{n_e \kappa} \right)^{-1} \quad (6)$$

where $Y_e = Z/A$, m_u is the atomic mass unit, F is the flux transmitted through the envelope, g_s the acceleration of gravity as measured at the surface, and S_e and n_e are the entropy and number density of the electron gas. Here, Z and A are the mean atomic number and mean atomic mass of the material. For partially ionized matter, Y_e is given by the product of Z/A and the ionized fraction.

We will further assume that the magnetic field is locally uniform and inclined relative to the vertical by the constant angle ψ . This approximation is valid provided that the field does not vary in direction or magnitude over the scale of the thickness of the envelope (h_E), *i.e.* $|B/\nabla B| \gg h_E$. For a multipole of order n , this is equivalent to $R/n \gg h_E$, where R is the stellar radius, which holds for $n \ll 100$. In this case, Equations 4 through 6 remain valid, but the thermal conductivity, κ , is now the sum of two contributions

$$\kappa = \kappa_{zz} \cos^2 \psi + \kappa_{yy} \sin^2 \psi \quad (7)$$

where the field is taken to point in the z direction. Provided that the crust is thin and the field does not vary significantly through the envelope, it can be shown that the multidimensional equations of thermal structure reduce to Equations 4 through 6 with κ given by the above relation (*e.g.* Paper I).

2.2. Thermodynamics, Equation of State and Conductivities

In an extremely strong magnetic field, the quantization of electron energies into Landau levels restricts the phase space of the otherwise free electron gas. Hernquist (1985) describes how to calculate the thermodynamic quantities necessary for integrating the structure of the neutron-star envelope. Further details of the thermodynamic calculations are also available in Heyl (1998).

Throughout the envelope, the heat is carried by electrons and photons. In the degenerate regime, electrons dominate the heat transfer and in the non-degenerate regime photons carry most of the heat.

2.2.1. Photon Conduction

As we argued in Paper I, for the envelopes that we will examine, photon conduction is impeded mainly by free-free interactions with the electron gas rather than by electron scattering. Regardless, corrections to the free-free opacity have a negligible influence on the flux-core temperature relation (Hernquist & Applegate 1984). Here, we will use the thermal conductivities tabulated by Silant'ev & Yakovlev (1980) and the analytic expressions of Pavlov & Yakovlev (1977).

2.2.2. Electron conduction

For the electron conductivities, we use the calculations of Hernquist (1984). Although the analytic formulae for the parallel conductivity derived by Potekhin & Yakovlev (1996) are convenient, corresponding results for the transverse heat flow are lacking; therefore, for consistency, we use the parallel and perpendicular thermal conductivities of Hernquist (1984).

The perturbations to the distribution function. The results of Hernquist (1984) take the form of perturbations to the distribution function (ϕ and Q) induced by a temperature gradient for various

scattering processes. The functions ϕ and Q are laborious to calculate. Hernquist (1984) gives fitting formulae for $n < 30$ at field strengths of $B = 10^{11}, 10^{11.5}, 10^{12}, 10^{12.5}, 10^{13}, 10^{13.5}$ and 10^{14} G. Additionally, to calculate the thermal structure of an envelope with an dipolar magnetic field, we have calculated the function ϕ at $B = 2 \times 10^{12}$ and 2×10^{13} G for $n < 30$ and at $B = 2 \times 10^{14}$ G for $n < 35$. Therefore, for fields $B \geq 2 \times 10^{14}$ G, the effect of the quantization of the electron phase space on the conductivity is included through the entire envelope.

When only one Landau level is filled, the functions ϕ and Q may be expressed analytically. In this limit, we use the following expressions

$$\phi_{ep}(\gamma; \beta) = \frac{1}{8}w [e^w E_1(w)]^{-1}, \quad (8)$$

$$Q_{ep}(\gamma; \beta) = \beta + \frac{4}{w} - 2e^w E_1(w) \quad (9)$$

$$\phi_{ei}(\gamma; \beta) = \frac{1}{8}w \left[\frac{1}{w + a_d} - \exp(w + a_d) E_1(w + a_d) \right]^{-1}, \quad (10)$$

$$Q_{ei}(\gamma; \beta) = \frac{1}{q_0^2} \left\{ [\beta(a_d + 1) + 2q_0^2] \exp(w + a_d) E_1(w + a_d) + \beta(a_d + 1)(q_0^2 + 1)e^{a_d} E_1(a_d) - \beta(2 + q_0^2) \right\} \quad (11)$$

where

$$q_0^2 = \gamma^2 - 1, \quad (12)$$

$$w = \frac{2q_0^2}{\beta}, \quad (13)$$

$$a_d = 0.15 \left(\frac{q_0^2}{2\beta} \right)^{1/3}, \quad (14)$$

and $E_n(x)$ is an exponential integral which is easily calculated and is defined by

$$E_n(x) = \int_1^\infty \frac{e^{-xt}}{t^n} dt, \quad x \geq 0, \quad n = 0, 1, \dots \quad (15)$$

Unquantized limit. To extend the conductivities beyond the maximum Landau level tabulated we use equations (186) through (189) of Hernquist (1984) to calculate the unmagnetized counterparts of ϕ and Q . In the liquid state we obtain,

$$\phi_{ei}(\gamma; \beta) = \frac{(\gamma^2 - 1)^3}{6\beta^3 \zeta^2 \Lambda_{ei}}, \quad (16)$$

$$Q_{ei}(\gamma; \beta) = \frac{8\Lambda_{ei}\gamma^2}{3}, \quad (17)$$

where the Coulomb logarithm Λ_{ei} is set to ensure continuity between the unquantized limit and the quantized calculations. It ranges from 1 at 10^{11} G to 0.55 at 10^{14} G. In the solid state we find

$$\phi_{ep}(\gamma; \beta) = \frac{(\gamma^2 - 1)^2}{3\beta^2 (\gamma^2 + 1)}, \quad (18)$$

$$Q_{ep}(\gamma; \beta) = \frac{4(\gamma^4 - 1)}{3\beta} \quad (19)$$

2.3. Numerical Integration of the Envelope

To determine the thermal structure of the neutron star envelope, we integrate Equations 4 through 6 using the photospheric boundary condition (*e.g.* Kippenhahn & Weigert 1990)

$$P_e = \frac{2}{3} \frac{g_s}{\tilde{\kappa}} = \frac{g_s \kappa \rho}{8\sigma T^3} \quad (20)$$

where $\tilde{\kappa}$ is the opacity and σ is the Stefan-Boltzmann constant. We omit Equation 5 from the system opting instead to solve for ζ by inverting $n_e(\zeta, \tau; \beta)$. The system is integrated with $\ln \rho$ as the independent variable using a Runge-Kutta method with adaptive step size control (Press et al. 1988). The properties of the envelope are calculated at 200 equally spaced steps in $\ln \rho$. A smaller stepsize results in an unacceptable accumulation of roundoff errors. The envelopes are integrated up to a density of $10^{10} \text{ g cm}^{-3}$.

3. Results

In this section we present the results of these numerical calculations. Specifically, we focus on several aspects of the envelopes: the thermal structure itself, the effect of dipolar fields on the moment of inertia of the envelope, the angular dependence of the flux for a constant field strength and the relationship between the transmitted flux and core temperature.

3.1. Thermal Structure

Parallel Conduction. If the quantization of the electron phase space is neglected, the magnetic field has no effect on the thermal conduction in the degenerate regime. We find that because this quantization cannot be neglected for $B > 10^{12} \text{ G}$, the magnetic field modifies the flux-core temperature relation, especially for relatively cool neutron stars. The case of parallel conduction has been treated in detail by Hernquist (1985) and Van Riper (1988), and we find similar results here.

Figure 1 depicts the temperature, chemical potential, entropy and thermal conductivity as a function of density through the crust at $T_{\text{eff}} = 10^6 \text{ K}$. The small discontinuity in the value of S_e at low densities occurs when the integrator switches from using the nondegenerate, nonrelativistic expression for $\zeta(n, \tau; \beta)$ to numerically solving for ζ . This discontinuity does not affect the integration through the nondegenerate regime.

The run of electron entropy as a function of density or depth through the envelope is not monotonic in the presence of a strong magnetic field. When one studies the total entropy, the nuclear contribution weakens this effect, but the total entropy still does attain a maximum as the first Landau level is being filled. This entropy inversion indicates that magnetized neutron star envelopes may be convectively unstable. However, a strong magnetic field also stabilizes a material against convection (Chandrasekhar 1961). To determine whether convection is indeed important requires further study

Our values for the core temperatures using the Hernquist (1984) conductivities are generally slightly higher for strong fields ($\sim 3\%$) than those obtained by Hernquist (1985) because we have varied Λ_{ei} to ensure continuity between the magnetized and the unmagnetized conductivities. A more substantial difference is apparent in the value of the thermal conductivity in the nondegenerate regime. Because the thermal conductivity is nearly a power law in this region, we expect the conductivity to be almost constant

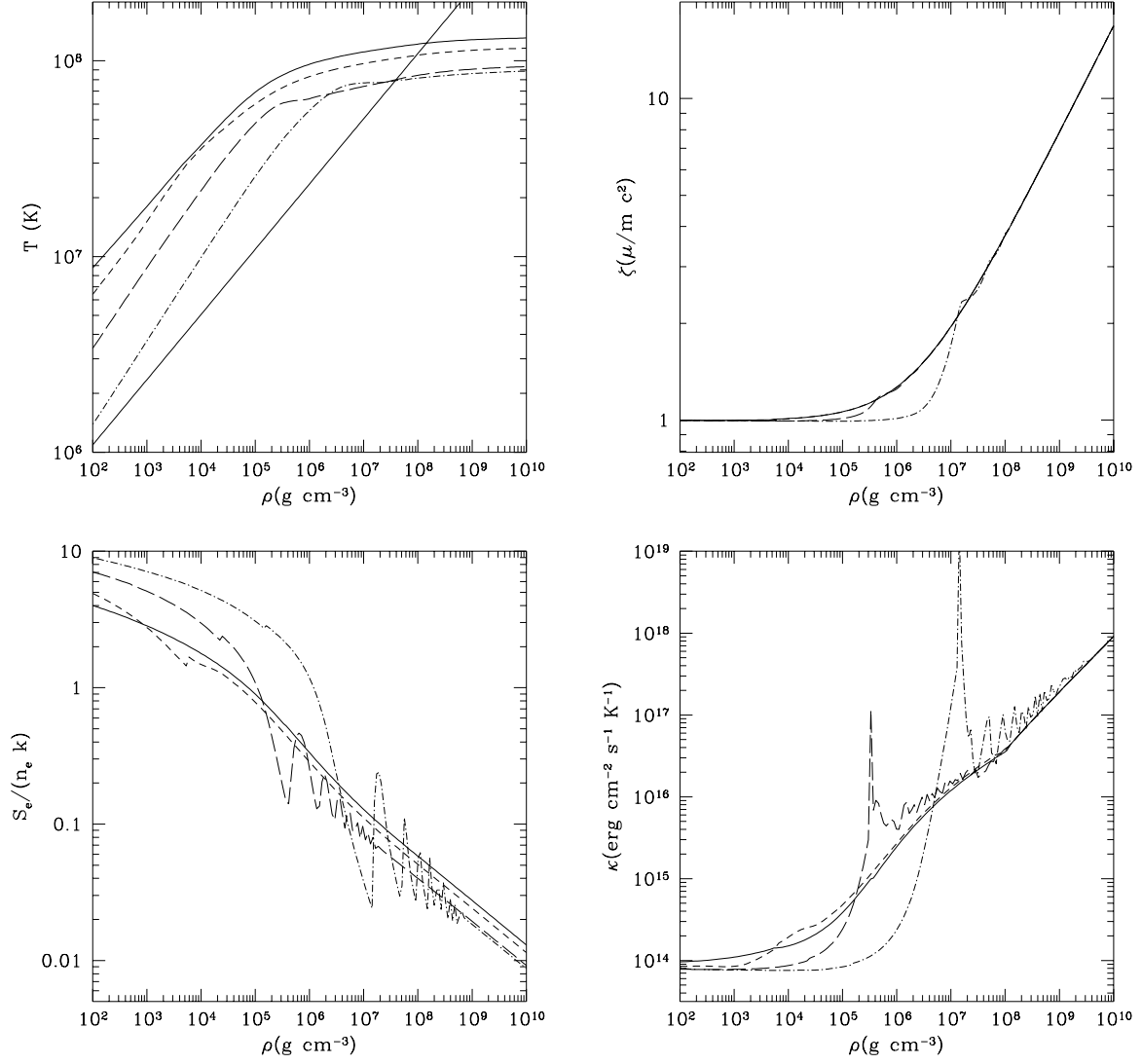


Fig. 1.— The thermal structure for a radial field at an effective temperature of 10^6 K. The solid curve traces the solutions for $B = 0$, the short dashed curve gives $B = 10^{12}$ G, the long dashed curve is 10^{13} G and the dot-dashed curve follows the $B = 10^{14}$ G solution. The solid line traces the solid-liquid phase transition in the $\rho - T$ plane.

along a solution here. According to Hernquist & Applegate (1984) for a unmagnetized atmosphere, the conductivity along a solution in the nondegenerate regime is

$$\kappa = \frac{\alpha + \delta}{\alpha} \frac{F}{g_s} \frac{Y_e k}{m_u} \quad (21)$$

where $\alpha = 2$ and $\delta = 6.5$ for free-free scattering. However, in the magnetized case we obtain,

$$\kappa = \frac{\alpha + \delta - 2}{\alpha} \frac{F}{g_s} \frac{Y_e k}{m_u}. \quad (22)$$

The thermal conductivity along a solution in the nondegenerate regime should be about 45 % larger for an unmagnetized envelope than for a magnetized envelope. This effect is apparent in Figures 1 and 2, but not in Figures 7 through 9 of Hernquist (1985). We find that the thermal conductivity in the nondegenerate region is given precisely by Equation 21 for the unmagnetized envelopes and by Equation 22 for the magnetized ones. The results of Hernquist (1985) for both magnetized and unmagnetized envelopes follow Equation 21. We are not certain of the origin of this discrepancy, but we suspect that it is due to inaccuracies in evaluating the conductivities in the nondegenerate limit. We expect that the results for cool envelopes which depend sensitively on conductivity in the nondegenerate region will differ between the work presented here and that of Hernquist (1985). Otherwise, the results for $T_{\text{eff}} = 10^6$ K agree well with those of Hernquist (1985).

Figure 2 depicts the physical conditions of the envelope as a function of density for effective temperatures of $10^{5.5}$ K (upper panels) and $10^{6.5}$ K (lower panels). In the colder envelope, the oscillations of the thermodynamic quantities owing to the quantization of the electron phase space is apparent. At higher and lower effective temperatures, the differences compared to the results of Hernquist (1985) are substantially larger. We obtain the solutions with higher core temperatures at $T_{\text{eff}} = 10^{5.5}$ K than Hernquist (1985) did because of the differences in the thermal conductivities in the nondegenerate region. Additionally, the relationship between the core temperature and magnetic field strength is complicated at such low effective temperatures. Specifically we find that for $T_{\text{eff}} \leq 10^{5.6}$ K the core temperature for an unmagnetized envelope is lower than in the magnetized case.

At $T_{\text{eff}} = 10^{6.5}$ K the situation is reversed. The envelopes studied here tend to yield cooler core temperatures than those studied by Hernquist (1985). For the hot envelopes with $B \lesssim 10^{13}$ G, the core temperature depends sensitively on the thermal conductivity in the liquefied region where more than thirty Landau levels are filled. In this region, unlike in Hernquist (1985), we have adjusted the value of Λ_{ei} to ensure continuity between the magnetized results and the unmagnetized limit. This yields slightly higher parallel conductivities for the liquid state, and consequently lower core temperatures.

In Figure 3, we compare the 10^{14} G models with the analytic models discussed in Paper I at $T_{\text{eff}} = 10^{5.5}, 10^6$ and $10^{6.5}$ K. At $T_{\text{eff}} = 10^6$ K, the numerical model has a core temperature 11 % cooler than the analytic treatment. The two approximations in the analytic model contribute errors that partly cancel. Since the analytic treatment assumes that either photon or electron conduction operates, it underestimates the conductivity in the semidegenerate region; consequently, in the degenerate regime, the analytic envelope is slightly hotter, and the resulting conductivity is larger than that of the numerical envelope at the same density. Above the density at which the first Landau level fills, the analytic treatment effectively assumes that the conductivity is infinite. Because the core temperature depends most sensitively on the conductivities in the semidegenerate region (*e.g.* Gudmundsson, Pethick & Epstein 1982), the net effect is that the numerical envelope at 10^6 K yields slightly higher core temperatures than the analytic treatment.

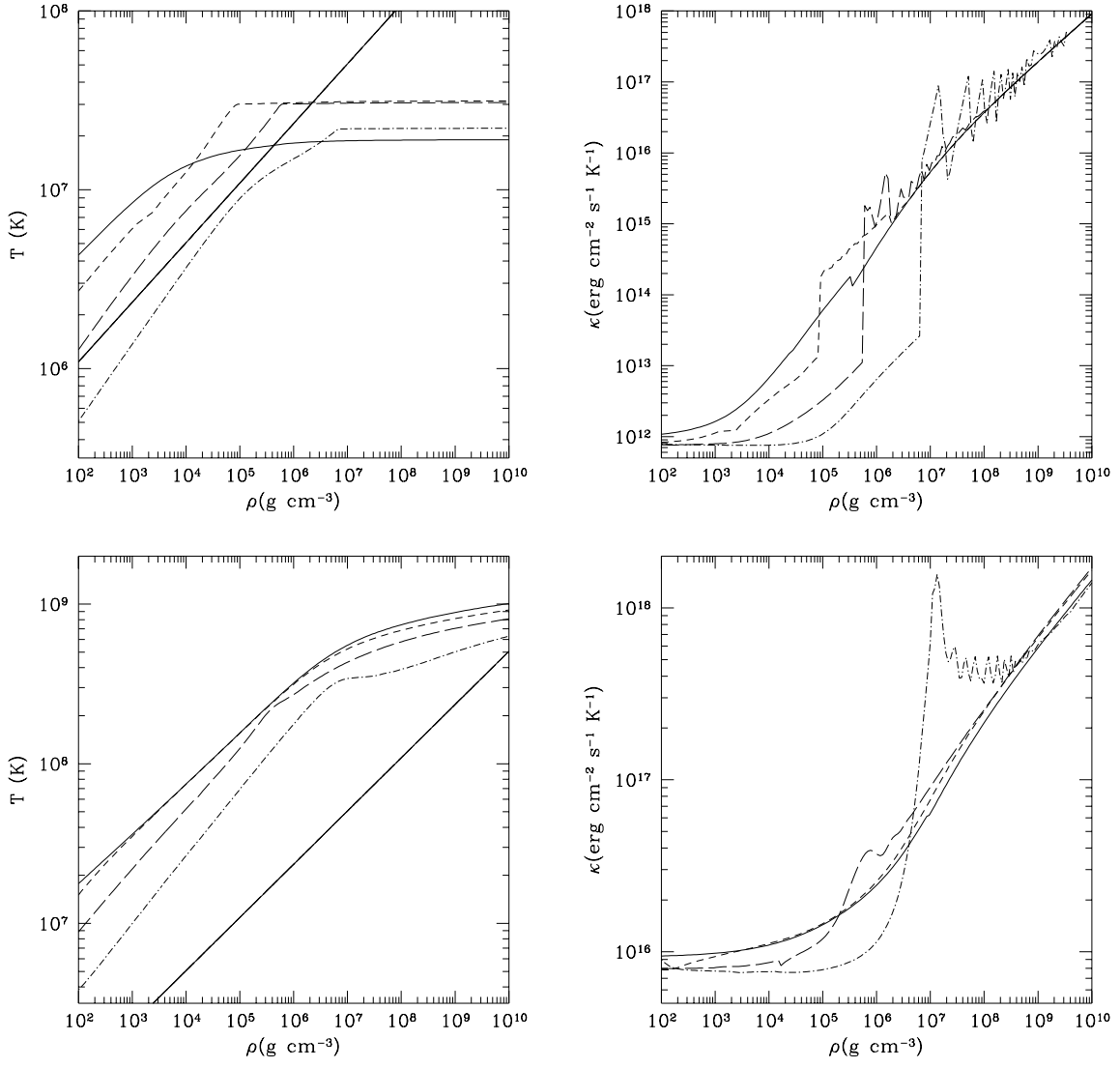


Fig. 2.— The thermal structure for a radial field at an effective temperature of $10^{5.5}$ K (upper panels) and $10^{6.5}$ K (lower panels). The lines follow the solutions for the same field strengths as in Figure 1.

At very low densities, the conductivity for the numerical solutions is higher than the constant conductivity of the analytic solution, because in the numerical treatment we start with the photospheric boundary condition rather than the radiative zero solution. The photospheric boundary condition assumes that $\tau = 2/3$ where $T = T_{\text{eff}}$. The zero solution puts $T = T_{\text{eff}}$ at $\tau = 4/3$; therefore, at a given low density, the numerical solutions are hotter than the analytic ones. However, the numerical solutions quickly relax to the radiative zero solution (*e.g.* Schwarzschild 1965).

For hotter and cooler effective temperatures, the cancellation among the errors introduced by the approximations is far less exact. At $T_{\text{eff}} = 10^{5.5}$ K the numerical treatment yields a core temperature 30 % hotter than the analytic model. At $T_{\text{eff}} = 10^{6.5}$ K the contribution to the insulation of the core from material with more than one Landau level filled is substantial and the core temperature estimate is 50 % higher for the numerical models than using the analytic treatment.

Perpendicular Conduction. Even classically, conduction perpendicular to the magnetic field is affected dramatically by a strong magnetic field. We again examine several magnetic field strengths. Figure 4 depicts the results for an effective temperature of $10^{5.5}$ K for perpendicular conduction. The core temperature for a fixed effective temperature varies dramatically with the magnetic field strength. The bulk of the effect is classical in nature, the magnetic field deflects the electrons from carrying heat away from the surface.

The quantization of the electron phase space is also manifest for the perpendicular case. Because the function $Q(\nu, \beta)$ diverges as a Landau level begins to fill, the conductivity increases dramatically near the start of each Landau level, and the run of temperature exhibits plateaux at these densities. As we shall find in the next subsections, perpendicular transport cannot be neglected an important range of effective temperatures and magnetic field strengths.

3.2. Angular Dependence

To examine the angular dependence of the flux transmitted through a uniformly magnetized envelope, we will take two routes. First, we use the method demonstrated in Figure 7 of Paper I and vary the effective temperature as a function of angle to shoot toward a fixed core temperature.

Figure 5 gives the outcome of this procedure. Both the $\cos^2 \psi$ rule and the best fit $a \cos^2 \psi + b \sin^2 \psi$ match the results to within 10 % of the total flux. Schaaf (1990b) presents the results of a set of two-dimensional calculations with a fitting function

$$\frac{T_{\text{eff}}(\psi)}{T_{\text{eff}}(0)} = \chi(\psi) = \chi(90^\circ) + [1 - \chi(90^\circ)] \cos^\alpha \psi. \quad (23)$$

Schaaf (1990b) studies field strengths up to 10^{12} G, so we assume that the parameters α and $\chi(90^\circ)$ for $T_{\text{eff}} = 10^6$ K follow a power law in the field strength for stronger fields. For $B = 10^{13}$ G, we obtain $\alpha = 0.48$ and $\chi(90^\circ) = 0.10$. This model is traced by the dashed line in Figure 5 and agrees to within 6.5 % of our results.

Bolstered by the success of the $\cos^2 \psi$ rule, we perform a second test in which the flux along the surface varies as $\cos^2 \psi$ and determine by how much the core temperature changes for several models. Figure 6 depicts the results of these calculations. A horizontal line for a given set of calculations would indicate adherence to the $\cos^2 \psi$ rule. Generally, the largest departure from the $\cos^2 \psi$ rule is where the heat is transmitted at large angles to the magnetic field direction.

We define a figure of merit for each value of the flux at $\psi = 0$ and magnetic field strength,

$$\Upsilon_u = \frac{1}{N} \sum_{i=1}^N \left| \frac{T_c(\psi_i) - T_c(0)}{T_c(0)} \right| \tag{24}$$

where u signifies an unweighted summation.

A large value of Υ_u indicates that conductivity perpendicular to the field lines is significant in determining the core temperature given the transmitted flux. Table 1 depicts the results for several field strengths and effective temperatures. We find two trends. For weak fields, the low effective temperature solutions follow the $\cos^2 \psi$ rule more closely than hotter envelopes. For strong fields, the trend is reversed.

From an observational point of view, the error in the total predicted luminosity of the object is more important. We weight the residuals by $\cos^2 \psi \sin \psi$. This neglects gravitational lensing and assumes the field distribution is uniform. We define

$$\Upsilon_L = \frac{\sum_{i=1}^N \cos^2 \psi \sin \psi \left| \frac{T_c(\psi_i) - T_c(0)}{T_c(0)} \right|}{\sum_{i=1}^N \cos^2 \psi \sin \psi} \tag{25}$$

where L signifies a luminosity-weighted summation. The values of Υ_L tend to be smaller than those of Υ_u because the weighting function is peaked at $\cos^2 \psi = 2/3$, approximately 35° , where the departure from the $\cos^2 \psi$ rule is small. We find that for effective temperatures near 10^6 K the $\cos^2 \psi$ dependence is followed. However, one must be wary in applying this rule for cool strongly magnetized envelopes where the quantization of the electron phase space increases the perpendicular conductivity dramatically or hot weakly magnetized ones where the classical relaxation time is no longer long compared to the relativistic cyclotron frequency.

3.3. Flux-Core-Temperature Relation

Figure 7 depicts the flux-core-temperature relation. We see that for very cool magnetized envelopes, the relationship departs from a power law. However, for $T_{\text{eff}} \geq 10^{5.7}$ K, the relationship is well fitted by a power law with root-mean-square residuals of less than 3%.

We have also examined envelopes with conduction perpendicular to the field for $T_{\text{eff}} = 10^{5.3}$ K, $10^{5.5}$ K and $10^{5.6}$ K, sufficient to determine the power-law flux-core-temperature relation for the perpendicular case. For higher effective temperatures, the core temperature exceeds 10^9 K. For such high core temperatures our assumption that the core is thermally relaxed breaks down (Nomoto & Tsuruta 1981). For lower

Table 1: Values of Υ in percent as a function of magnetic field and effective temperature

B (G)	Υ_u			Υ_L		
	log T_{eff}			log T_{eff}		
	5.5	6.0	6.5	5.5	6.0	6.5
10^{12}	0.86	8.4	21.	1.1	3.7	16.
10^{13}	0.74	4.9	6.1	0.54	2.4	1.9
10^{14}	12.	7.2	3.5	7.0	4.0	2.0

effective temperatures, the details of the equation of state at low densities become important, *i.e.* Coulomb corrections (*e.g.* Van Riper 1988).

We fit the flux-core-temperature relation with a power law of the form,

$$T_{c,7} = T_{0,7} T_{\text{eff},6}^{\alpha}. \tag{26}$$

Table 2 presents the results of the fitting. The slope of flux-core-temperature relation for the parallel case is approximately that found in the analytic treatment of Paper I (cf. equations 36 and 37 in Paper I). However, the relationship with magnetic field strength is a much shallower power law than found earlier.

3.4. Dipole Fields

It is straightforward to construct the effective temperature distribution for a dipole field by interpolating the flux-core-temperature relation as function of field strength and field inclination. However, determining the thermal structure in this manner is less trivial. The goal is to determine if an intense magnetic field can cause the envelope to become oblate through its effect on heat transport, so we will examine perpendicular and parallel transport for a field strength at the pole of 2×10^{14} G by recalculating an envelope solution and matching the core temperature at the pole and the equator. For illustration we choose $T_{\text{eff}}(\psi = 0) = 10^{6.4}$ K which yields a core temperature of 4×10^8 K. Along the magnetic equator, substantially less heat flows through the envelope. Here, $T_{\text{eff}} \approx 10^{5.38}$ K.

Figure 8 depicts the two solutions. The run of temperature with density is substantially different for the two solutions, so we would expect that the moment of inertia of the envelope at the pole would differ from that at the equator. To first order, the moment of inertia of the envelope depends on the total mass of the envelope and the mass weighted mean radius of the envelope. The envelope is about 0.7 % thinner and less massive at the equator than at the poles. For a neutron star with $R = 10^6$ km and $I = 1.4 \times 10^{45}$ g cm², the moment of inertia of the envelope at the pole differs by a factor of 1.2×10^{-3} relative to the equatorial value. This difference results in a relative difference in the moment of inertia along and perpendicular to the magnetic field of 10^{-11} .

Near the magnetic equator of the neutron star, an equatorial ice band floats above the ocean. The ice band extends to a density of 1.6×10^6 g cm⁻³ and a depth of approximately 70 cm while the surrounding ocean reaches $\rho \sim 5 \times 10^9$ g cm⁻³ and a depth of nearly 300 m. This ice band forms because the conductivity in the nondegenerate magnetized envelope is nearly constant; therefore $T \propto \rho^{4/9}$ and $\Gamma \propto \rho^{-1/9}$. The envelope tends to melt as the density increases. For any significant ice band to form the region of the neutron star must be insulated from the core by a tangential magnetic field, *i.e.* near the magnetic equator. For free-free opacity without a magnetic field, we obtain $T \propto \rho^{4/13}$ and $\Gamma \propto \rho^{1/39}$ and this effect is absent.

Table 2: Power-law parameters for the flux-core-temperature relation.

B (G)	$T_{\parallel,0,7}$	α_{\parallel}	$T_{\perp,0,7}$	α_{\perp}
0	13.3	1.76		
10^{12}	12.0	1.76	52.9	1.21
10^{13}	10.1	1.76	123.	1.16
10^{14}	9.35	1.62	213.	1.17

4. Discussion

The calculations here are patterned after those of Hernquist (1985), and for the case of parallel conduction we reproduce his results with a few exceptions. Because we use the formulae of Pavlov & Yakovlev (1977) to extrapolate the free-free opacity in the non-degenerate regime beyond the tabulations of Silant’ev & Yakovlev (1980), we find different thermal structure in the nondegenerate region than did Hernquist (1985), who extrapolated the calculations of Silant’ev & Yakovlev (1980) directly; consequently, for those especially cool envelopes whose core temperatures depend sensitively on these opacities, we find that our envelopes transmit less flux for a given core temperature. To calculate the thermal conductivity due to electron transport, we have extrapolated the tabulations of Hernquist (1984) for $n \geq 30$ in manner which maintains continuity between the magnetized and unmagnetized limits. Specifically, this results in a slightly higher electron conductivity for $n \geq 30$ than Hernquist (1985) used. We find that for high effective temperatures, more flux is transmitted for a given core temperature than Hernquist (1985) found.

By examining transport oblique and perpendicular to the field direction, we have extended the earlier work of Hernquist (1985) and Van Riper (1988) into two-dimensions, and the work of Schaaf (1990b) to more intense magnetic fields and more complicated field geometries. Schaaf (1990b) solves the thermal structure equation in two dimensions using the conductivities of Schaaf (1988) for $B \leq 10^{11}$ G. Using the same set of conductivities, Schaaf (1990a) treats the cases of parallel and perpendicular transport using a plane-parallel approximation for $B \leq 10^{13}$ G.

Rather than solve the two-dimensional thermal structure equations directly, we have argued in Paper I that the plane-parallel approximation holds for the relatively thin envelopes of neutron stars. The slope of the flux-core-temperature relation for the longitudinal case agrees with the fit of Schaaf (1990a) to within 15 %, and the normalization agrees to within 8 %. Furthermore, Schaaf (1990a) also found an upturn in the flux-core-temperature relation for magnetized envelopes with low effective temperatures. For the transverse case, we find that the flux-core-temperature relation has a similar slope as Schaaf (1990a) but our models tend to have higher core temperatures.

Our results do not extend beyond an effective temperature of $10^{6.5}$ K (longitudinal case) and $10^{5.6}$ K (transverse case). For higher effective temperatures the core temperature exceeds 10^9 K, and it is unlikely that the core has relaxed thermally yet (Nomoto & Tsuruta 1981).

Schaaf (1990b) summarizes the results of the two-dimensional calculations in terms of fitting functions (Equation 23). In this notation we have examined the applicability of two models. Both models have $\alpha = 0.5$. The first fixes $\chi(90^\circ) = 0$, the $\cos^2 \psi$ rule, and the second allows $\chi(90^\circ)$ to vary, the $a \cos^2 \psi + b \sin^2 \psi$ rule.

The two works have only the $T_{\text{eff}} = 10^6$ K with $B = 10^{12}$ G model in common, but our results assume a given flux rule and determine the change in core temperature. However, we find that the model $T_{\text{eff}} = 10^{5.5}$ K and $B = 10^{12}$ G is well fit by the $\cos^2 \psi$ rule. Using the Schaaf (1990b) interpolation formulae, we obtain $\alpha = 0.44$ and $\chi(90^\circ) = 0.32$ which yields more flux at large values of ψ than we found. We also extrapolated the interpolation formulae of Schaaf (1990b) to 10^{13} G for $T_{\text{eff}} = 10^6$ K and find agreement within 7%.

Several directions for further work stand out. The equation of state at low densities may be affected by Coulomb corrections. Van Riper (1988) found that Coulomb corrections play an important role for effective temperatures less than 6×10^5 K at 10^{14} G. Their contribution sets in at lower effective temperatures for more weakly magnetized envelopes. The prescription of Van Riper (1988) for including Coulomb corrections

resulted in negative pressures at low densities. Thorolfsson et al. (1997) have developed a Thomas-Fermi technique which accounts for the quantization of the electron phase space which may be applied to envelope calculations without encountering the difficulties that Van Riper (1988) found.

In the degenerate regime where electron conduction dominates, the conductivities are still uncertain. Potekhin & Yakovlev (1996) have derived convenient analytic formulae to calculate the longitudinal transport coefficients. Potekhin & Yakovlev (1996) make slightly different approximations from other workers. They include Debye and electron screening in the fluid phase and the Debye-Waller factor in solid state. This factor tends to increase the conductivity over a wide range of temperatures and densities (Itoh et al. 1984; Potekhin & Yakovlev 1996). With an equally complete treatment of the transverse conductivities, this work could be extended reliably into a wider range of effective temperatures and magnetic field strengths.

To connect these results with recent observations of isolated neutron stars (*e.g.* Greiveldinger et al. 1996; Possenti, Mereghetti & Colpi 1996; and see Table 1 of Paper I), we must calculate how a magnetized atmosphere determines the emergent spectra from various locations on the neutron star (Pavlov et al. 1994; Pavlov et al. 1996; Rajagopal, Romani & Miller 1997), and convolve these spectra with the effects of gravitational self-lensing to determine the portion of the neutron star visible as a function of rotational phase (Page 1995; Paper I).

5. Conclusion

We have presented a series of numerical models of neutron star envelopes calculated in the plane-parallel approximation for $B = 10^{12}$ to 10^{14} G, $T_{\text{eff}} = 10^{5.3}$ to $10^{6.5}$ K, and for several inclination angles of the magnetic field. We find agreement with earlier one and two-dimensional calculations, and verify that the flux along the surface is approximately proportional to the square of the cosine of the inclination angle for neutron stars with $T_{\text{eff}} \sim 10^6$ K. For hotter and cooler envelopes, this rule provides a poorer approximation.

With the imminent launch of the AXAF observatory, understanding the properties of neutron star envelopes is crucial to interpreting the observations and constraining models of neutron stars, and thereby the properties of nuclear matter. The neutron star envelope determines the thermal flux from the surface at a given core temperature. The numerical models presented here will allow a more accurate translation of the observed emission from neutron star surfaces into knowledge of their interiors. When combined with calculations of radiative transfer through strongly magnetized atmospheres, our models for the thermal structure of neutron star envelopes will make it possible to examine the influence of the field strength and surface gravity and composition on the spectra of isolated cooling neutron stars with unprecedented detail.

We thank the referee, V.A. Urpin, for comments that improved the presentation. The work was supported in part by a National Science Foundation Graduate Research Fellowship, Cal Space grant CS-12-97 and a Lee A. DuBridge postdoctoral scholarship.

REFERENCES

- Chandrasekhar, S. 1961, *Hydrodynamic and Hydromagnetic Stability*, Clarendon Press, Oxford
- Greiveldinger, C. *et al.* 1996, *ApJL*, **465**, 35.

- Gudmundsson, E. H., Pethick, C. J. & Epstein, R. I. 1982, *ApJL*, **259**, 19.
- Hernquist, L. 1984, *ApJS*, **56**, 325.
- Hernquist, L. 1985, *MNRAS*, **213**, 313.
- Hernquist, L. & Applegate, J. H. 1984, *ApJ*, **287**, 244.
- Heyl, J. S. 1998, *Ph.D. thesis*, University of California at Santa Cruz.
- Heyl, J. S. & Hernquist, L. 1998, *MNRAS*, in press (Paper I).
- Itoh, N., Yasuharu, Kohyama, Matsumoto, N. & Seki, M. 1984, *ApJ*, **285**, 758.
- Kippenhahn, R. & Weigert, A. 1990, *Stellar Structure and Evolution*, Springer, Berlin
- Nomoto, K. & Tsuruta, S. 1981, *ApJL*, **250**, 19.
- Page, D. 1995, *ApJ*, **442**, 273.
- Pavlov, G. G., Shibano, Y. A., Ventura, J. & Zavlin, V. E. 1994, *A&A*, **289**, 837.
- Pavlov, G. G. & Yakovlev, D. G. 1977, *Astrophysics*, **13**, 89.
- Pavlov, G. G., Zavlin, V. E., Trümper, J. & Neuhäuser, R. 1996, *Multiwavelength observations of isolated neutron stars as a tool to probe the properties of their surfaces*, astro-ph/9609097
- Possenti, A., Mereghetti, S. & Colpi, M. 1996, *A&A*, **313**, 565.
- Potekhin, A. Y. & Yakovlev, D. G. 1996, *A & A*, **314**, 341.
- Press, W. H., Flannery, B. P., Teukolsky, S. A. & Vetterling, W. T. 1988, *Numerical Recipes in C*, Cambridge Univ. Press, Cambridge, first edition
- Rajagopal, M., Romani, R. W. & Miller, M. C. 1997, *ApJ*, **479**, 347.
- Schaaf, M. E. 1988, *A&A*, **205**, 335.
- Schaaf, M. E. 1990a, *A&A*, **227**, 61.
- Schaaf, M. E. 1990b, *A&A*, **235**, 499.
- Schwarzschild, M. 1965, *Structure and Evolution of the Stars*, Dover, New York
- Silant'ev, N. A. & Yakovlev, D. G. 1980, *Astrophys. Sp. Sci.*, **71**, 45.
- Thorolfsson, A., Rögnvaldsson, O. E., Yngvason, J. & Gudmundsson, E. H. 1997, *Thomas-Fermi Calculations of Atoms and Matter in Magnetic Neutron Stars II: Finite Temperature Effects*, astro-ph/9711091
- Van Riper, K. A. 1988, *ApJ*, **329**, 339.

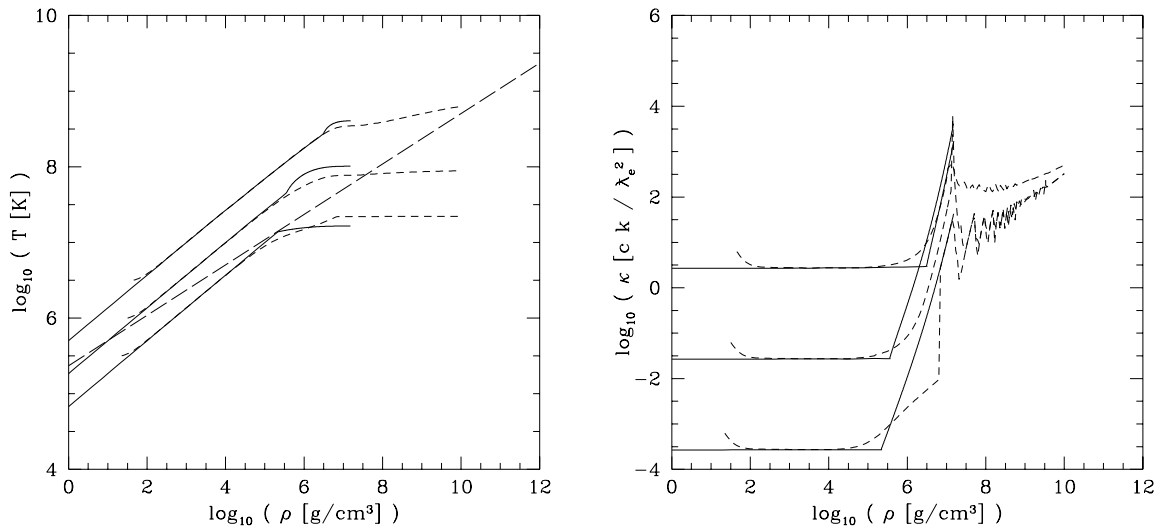


Fig. 3.— Comparison of analytic and numerical envelope solutions for a radial field. From top to bottom, the curves follow the solutions for $T_{\text{eff}} = 10^{5.5}$ K, 10^6 K and $10^{6.5}$ K. The left panel depicts the dependence of temperature on density through the envelope of the neutron star. The right panel gives the run of conductivity with density. The solid lines trace the analytic solutions and the dashed follows the numerical results.

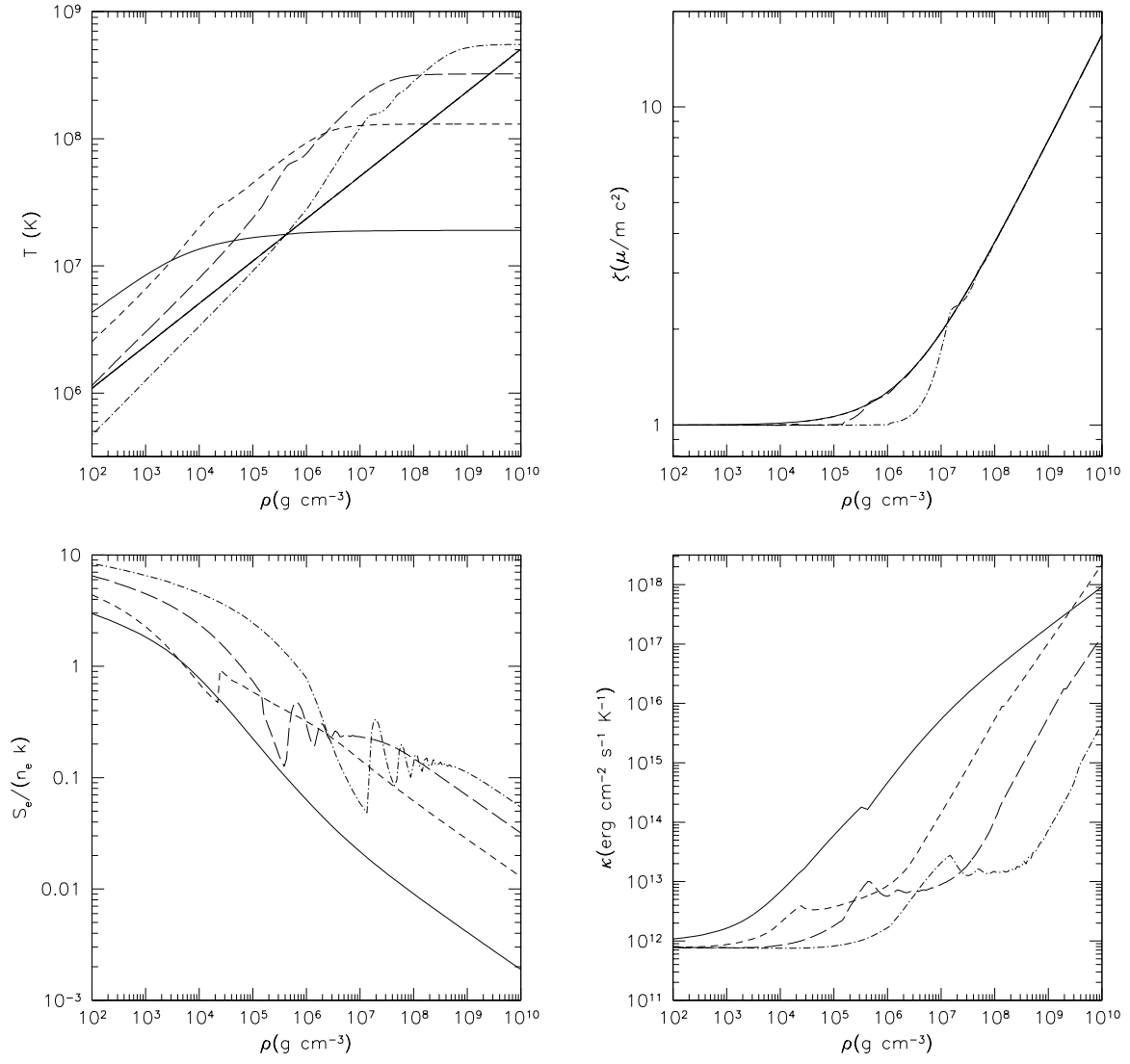


Fig. 4.— The thermal structure for a tangential field at an effective temperature of $10^{5.5}$ K. The lines follow the solutions for the same field strengths as in Figure 1.

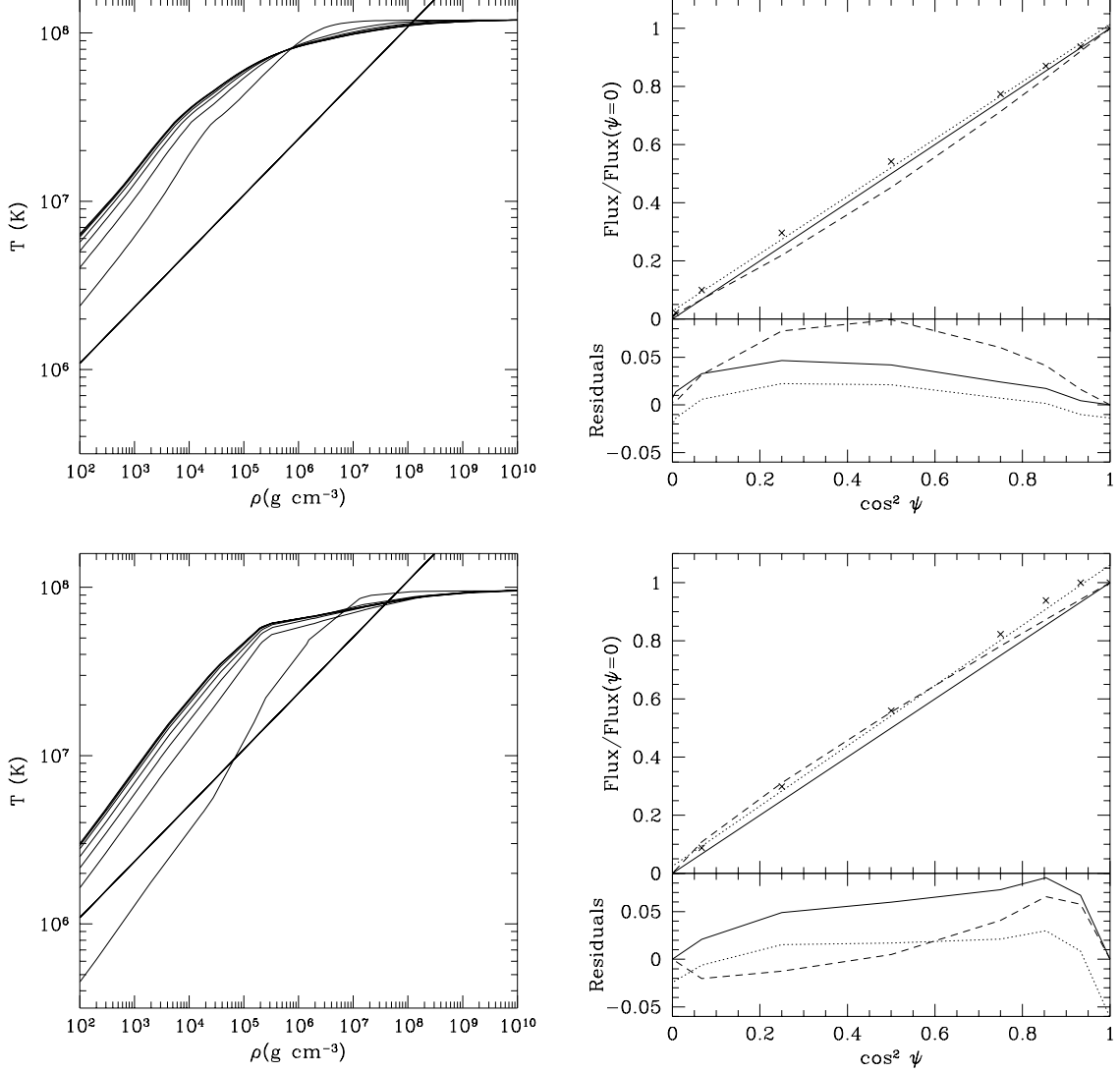


Fig. 5.— Results of a numerical two-dimensional calculation for $B = 10^{12}, 10^{13}$ G at $T_{\text{eff}} = 10^6$ K for $\psi = 0$. The upper panels present the results for the weaker field strength. The left panels give $T(\rho)$ for the various models. The right panels compare the flux distribution (crosses) with the $\cos^2 \psi$ rule. The lower solid line gives the $\cos^2 \psi$ rule and the upper dotted line traces the best fit model of the form $a \cos^2 \psi + b \sin^2 \psi$. Here, $a = 1.02$ and $b = 0.0264$ for 10^{12} G, $a = 1.06$ and $b = 0.0245$ for 10^{13} G. The dashed line traces the results of Schaaf (1990b) (extrapolated using a power law to $B = 10^{13}$ G).

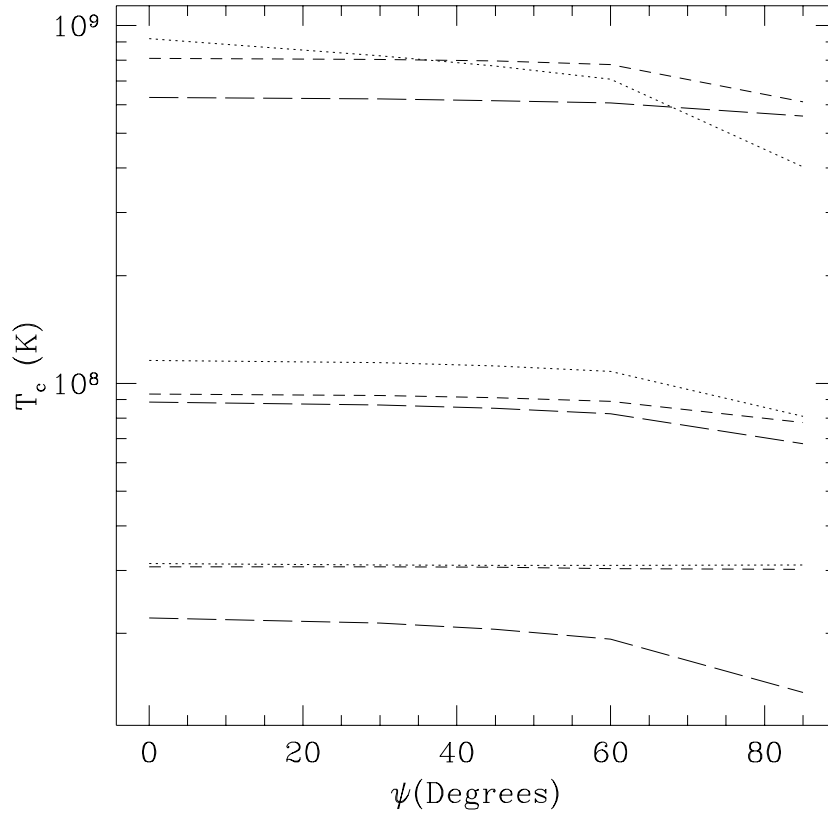


Fig. 6.— The core temperature as a function of angle for fluxes that follow the $\cos^2 \psi$ rule. The lower lines are for $T_{\text{eff}}(\psi = 0) = 10^{5.5}$ K, and middle lines follow the 10^6 K solutions, and the upper lines trace the $10^{6.5}$ K results. The lines follow the solutions for the same field strengths as in Figure 1.

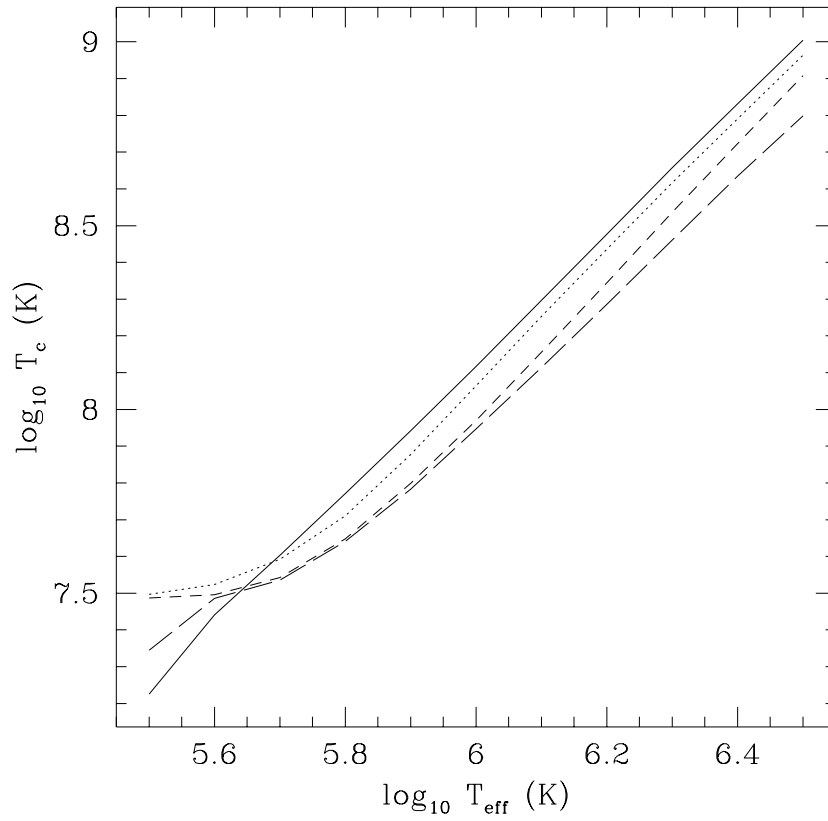


Fig. 7.— The flux-core-temperature relation as a function of magnetic field strength for a radial field. The lines follow the solutions for the same field strengths as in Figure 1.

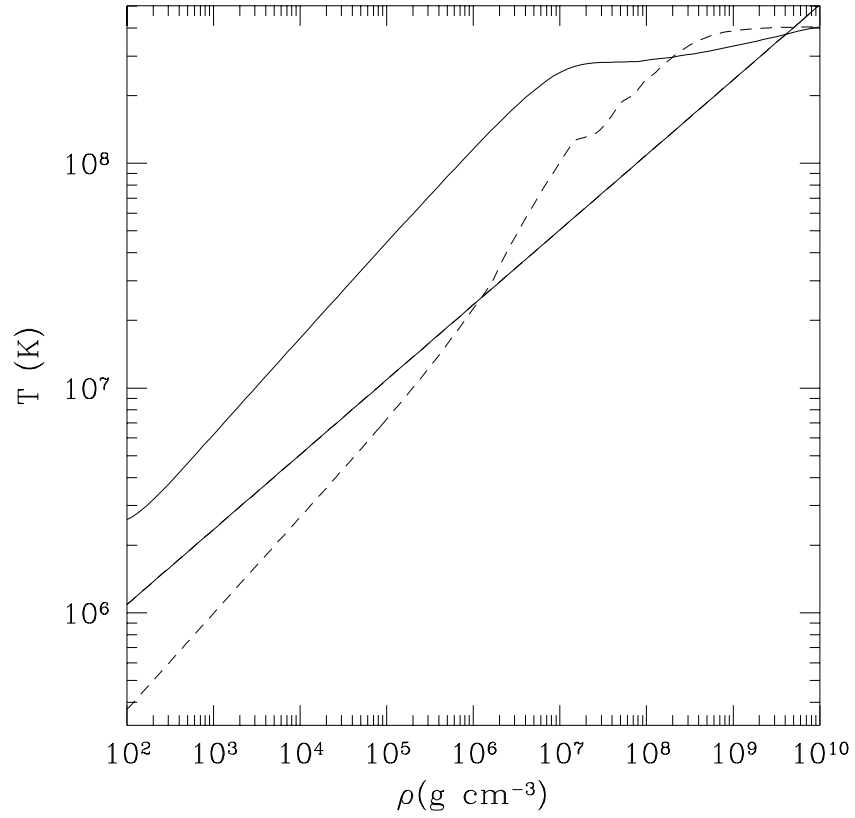


Fig. 8.— The thermal structure for a dipole field configuration ($B_p = 2 \times 10^{14}$ G). The solid curve traces the solution at the pole, and the dashed curve gives the results at the equator. The solid straight line follows the liquid-solid phase boundary.